Speed Fuzzy Control Applied to Autonomous Electric Vehicles

ÍTALO A. SOUZA-DE-ASSIS, RENAN OLIVEIRA, MARCELO A. C. FERNANDES*
Federal University of Rio Grande do Norte (UFRN)
Department of Computer Engineering and Automation (DCA)
59078-970, Natal, RN
BRAZIL
*Corresponding author: mfernandes@dca.ufrn.br

Abstract: A cruise control system for autonomous electric vehicles (AEVs) is presented, based on fuzzy logic. The proposed technique uses three fuzzy systems that act in parallel during three kinetic states of the vehicle: acceleration, moving, and braking. Validation of the procedure used longitudinal simulations of a vehicle powered by a permanent magnet direct current motor. The results indicated that the control system performed satisfactorily, and could be used in AEV applications.

Key–Words:Fuzzy Logic, Autonomous Electric Vehicle, Cruise Control

1 Introduction

Research has shown that the performance achieved using intelligent controllers exceeds that of traditional controllers. Control algorithms based on artificial neural networks (ANNs) and/or fuzzy logic offer substantial gains over conventional techniques such as the PID [1, 2], as a result of which there is increasing interest in the development of intelligent control systems. In particular, there is growing commercial awareness of the possible application of these systems in autonomous vehicles, where they could help to reduce accidents and improve the comfort of the occupants [3, 4].

A further consideration relates to the capacity of highways, since with reliable sensors and automation, improvements could be made over human reaction times and safe distances between vehicles could be shortened [5]. An important point is that intelligent control systems for AEVs could be rapidly implemented without requiring major investments in infrastructure [6–9].

Processes based on fuzzy logic are amongst the most efficient intelligent control systems, enabling the rapid development of controllers for temporally variable nonlinear systems [10]. An important advantage of fuzzy control is that there are many cases where binary values (true or false, connected or disconnected, etc.) are unable to provide a good description of the situation. These cases require a scale whereby the variables can be assigned intermediate values [10]. This can be achieved using fuzzy logic in controllers [1, 11–13].

Fuzzy controllers have already been used for speed control of autonomous vehicles, and have been shown to provide performance superior to that of conventional PID techniques, especially concerning errors, vibration, and robustness [14]. A fuzzy strategy was found to offer advantages over a neuro-fuzzy approach or PI controllers applied to autonomous vehicles [15]. Several studies have described the development of autonomous vehicle speed controllers based on fuzzy logic [16–19].

There are two main problems to be addressed in the development of autonomous vehicles: (i) lane keeping, and (ii) longitudinal headway [20]. The latter has been the subject of research for at least 40 years, and there are many theoretical studies reported in the literature [21–24].

The objective of the present work was to design a longitudinal cruise control system for AEVs, based on fuzzy logic. Different to the work that has been published previously, the proposed system uses three sets of fuzzy rules that act in parallel for three kinetic states of the vehicle: acceleration, moving, and braking. The goal of the system was to be able to smoothly accelerate the vehicle until it reached a predetermined cruising speed (the reference speed) within a set time (the reference time), and then maintain this speed during movement of the vehicle. The fuzzy controller should also be able to reduce the speed of the vehicle without any abrupt changes, so that the vehicle halts at a predetermined distance from the starting point. This type of system could be used in autonomous vehicles for transportation of products sensitive to abrupt movements, where the route is known in advance, with previous programming of acceleration, cruise speed, and braking.

Details of the electric vehicle model used are provided in Section 2. A description of the control strategy used in each stage of the vehicle kinetics is given in Section 3. A description of the specific characteristics of the simulation is given in Section 4, including the route, the values selected for the different parameters, and the results obtained. Finally, an evaluation of the proposed scheme and its performance is provided in Section 5.

2 Modeling of the AEV

The electric vehicle used in the simulations was represented by a longitudinal dynamics model with a permanent magnet direct current (PMDC) motor [25–27]. The objective of the controller was to adjust the voltage in order to maintain the speed of the vehicle within the given specifications.

The dynamics of the PMDC motor (Figure 1) were modeled by an equation representing the electrical aspects and another equation representing the mechanical aspects, as described previously [27]. The differential equation used to model the electrical part can be described by

$$v_a(t) = R_a i_a(t) + L_a \frac{di_a(t)}{dt} + v_i(t), \qquad (1)$$

where $v_a(t)$, $i_a(t)$, R_a and L_a are the voltage in volts (V), the current in amps (A), the resistance in ohms (Ω), and the inductance in henrys (H), respectively, in the armature of the PMDC motor, and $v_i(t)$ is the voltage induced in the rotor terminals (V). The mechanical part was modeled using the expression

$$J_m \frac{d\omega_m(t)}{dt} = \tau_m(t) - B_m\omega_m(t) - \tau_c(t), \qquad (2)$$

where J_m is the moment of inertia of the rotor (Kg.m^2), B_m is the viscosity constant (N.m.s), $\omega_m(t)$ is the angular velocity of the rotor (rad/s), $\tau_m(t)$ is the torque generated by the motor (also known as the magnetic torque) (N.m), and $\tau_c(t)$ is the torque required to move the load (N.m).

In PMDC motors, the magnetic torque, $\tau_m(t)$, is directly proportional to the current in the armature, $i_a(t)$, so that

$$\tau_m(t) = K_\tau i_a(t), \qquad (3)$$

and the angular velocity, $\omega_m(t)$, is directly proportional to the induced voltage, $v_i(t)$, as described by

$$v_i(t) = K_\omega \omega_m(t) \qquad (4)$$

where K_τ is the torque constant (N.m/A) and K_ω is the velocity constant (V/rad/s) of the PMDC motor [27].

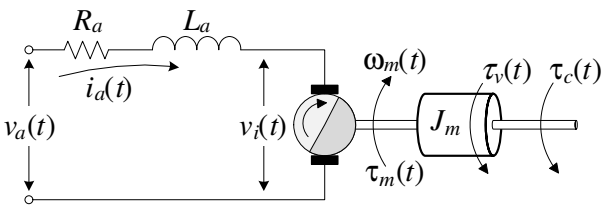

Figure 1: Electromechanical schematic of the PMDC motor.

The longitudinal vehicle model, illustrated in Figure 2, can be described by the expression

$$M\frac{dx(t)}{dt} = f_t(t) - f_a(t), \qquad (5)$$

where M is the mass of the vehicle (Kg), $x(t)$ is the linear velocity of the vehicle (m/s), $f_t(t)$ is the traction force of the vehicle (N), and $f_a(t)$ is the friction force (N).

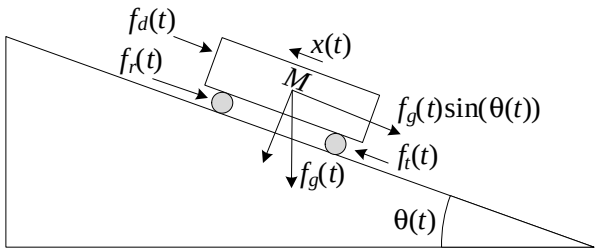

Figure 2: Schematic of the longitudinal vehicle model.

According to [25], the friction force, $f_a(t)$, can be expressed as

$$f_a(t) = f_d(t) + f_r(t) + f_g(t)\sin(\theta(t)), \qquad (6)$$

where $f_d(t)$ is the aerodynamic friction force (N), $f_r(t)$ is the rolling resistance force (N), $f_g(t)$ is the gravitational force (N), and $\theta(t)$ is the inclination angle of the plane on which the vehicle is located.

The aerodynamic friction can be described by

$$f_d(t) = \frac{1}{2}\rho C_d A_{fr} x^2(t), \qquad (7)$$

where ρ is the density of air, C_d is the aerodynamic drag coefficient, and A_{fr} is the frontal area of the vehicle (m^2). The rolling resistance force can be described by

$$f_r(t) = Mg\left(C_0 + C_1 x^2(t)\right), \qquad (8)$$

where C_0 and C_1 are the rolling coefficients and g is the acceleration due to gravity (m/s^2). Finally, the gravitational force is given by

$$f_g(t) = Mg. \tag{9}$$

The coupling between the PMDC motor and the vehicle was modeled by a simple system of gears positioned parallel to the rear axle of the vehicle, described by

$$\tau_a(t) = k\tau_m(t), \tag{10}$$

where k is the gear ratio, and

$$f_a(t) = \frac{\tau_a(t)}{r} \tag{11}$$

where r is the radius of the wheel of the vehicle (m).

3 Control strategy

The proposed control strategy uses three fuzzy systems acting in parallel for three kinetic states of the vehicle (acceleration, moving, and braking). This division increases the precision with which the speed of the AEV can be controlled, enabling smoother responses during acceleration and braking as well as a more stable speed during moving. The three systems are governed by a decision-making strategy that employs two reference parameters: t_{ref}, which determines the acceleration state time, and l_{ref}, which establishes the distance to the final destination in order to initiate the braking state. In addition to this information, the control strategy uses two additional parameters, namely the distance that the vehicle must cover to the final destination, l_{end}, and the reference speed, x_{ref}, which is the speed that the vehicle should reach at the end of the acceleration state and then maintain during the moving state. A detailed block diagram of the control strategy is provided in Figure 3.

The fuzzy system responsible for the acceleration state, $\text{FS}_d(\cdot)$, can be described by

$$v_d(t) = \text{FS}_d\left(e_x\left(t\right)\right) \tag{12}$$

where $v_d(t)$ is the voltage (V) applied to the motor during the acceleration state, and $e_x\left(t\right)$ is the error between the reference speed, x_{ref}, which is desired at the end of the acceleration state, and the actual speed of the vehicle, described by

$$e_x(t) = x_{ref} - x(t). \tag{13}$$

The fuzzy system associated with the moving state, $\text{FS}_m(\cdot)$, is characterized by

$$v_m(t) = \text{FS}_m\left(e_x\left(t\right), de_x\left(t\right)\right), \tag{14}$$

where $v_m(t)$ is the voltage (V) applied to the motor during the moving state, and $de_x\left(t\right)$ is the derivative of the error $e_x\left(t\right)$. Finally, the fuzzy system used to characterize the braking state, $\text{FS}_b(\cdot)$, is described by

$$v_b(t) = \text{FS}_b\left(e_x\left(t\right), l\left(t\right)\right), \tag{15}$$

where $v_b(t)$ is the voltage (V) applied to the motor during the braking state, and $l(t)$ is the distance (m) travelled by the vehicle to the final destination.

The decision strategy used to select one of the three systems (FS_d, FS_m and FS_b, described by Eq. (12), Eq. (14), and Eq. (15), respectively) is characterized by

$$v_a(t) = \begin{cases} v_d(t) & \text{if } t \leq t_{ref} \text{ and } l(t) < l_{end} - l_{ref} \\ v_m(t) & \text{if } t > t_{ref} \text{ and } l(t) < l_{end} - l_{ref} \\ v_b(t) & \text{if } t > t_{ref} \text{ and } l(t) \geq l_{end} - l_{ref} \end{cases}. \tag{16}$$

The input and output membership functions and the set of rules associated with each of the three fuzzy systems are described in detail in Sections 3.1, 3.2 and 3.3. They are based on a subjective analysis of the action of a human driver, with the aim of achieving smooth acceleration and braking, as well as a stable speed in a longitudinal route with random ascents and descents.

The limits of the membership functions associated with the output variables $v_d(t)$, $v_m(t)$ and $v_b(t)$ were selected for motors with a nominal armature voltage, $v_a^{nom}(t)$, of 220V. However, these limits could be easily readjusted for motors with other values of $v_a^{nom}(t)$.

3.1 Fuzzy system for acceleration

The fuzzy system for acceleration, $\text{FS}_d(\cdot)$, can be described by the membership functions shown in Figures 4 and 5. The input variable, $e_x\left(t\right)$, s represented by a group of seven linguistic variables with triangular and trapezoidal membership functions, as illustrated in Figure 4. In the case of the output variable, $v_d(t)$, only three linguistic variables with triangular membership functions are used (Figure 5). Table 1 details the set of fuzzy rules used in the Mamdani inference process in order to relate the input variable, $e_x\left(t\right)$, with the output variable, $v_d(t)$.

Since the objective of the $\text{FS}_d(\cdot)$ system is to achieve smooth acceleration, the membership functions of the output variable, $v_d(t)$, are slightly above the nominal average armature voltage of the vehicle, $v_a^{nom}(t)$, which in the present case is 220V. This strategy enables the motor voltage during acceleration to be limited to the range

$$v_d^{min}(t) \leq v_d(t) \leq v_d^{max}(t) \tag{17}$$

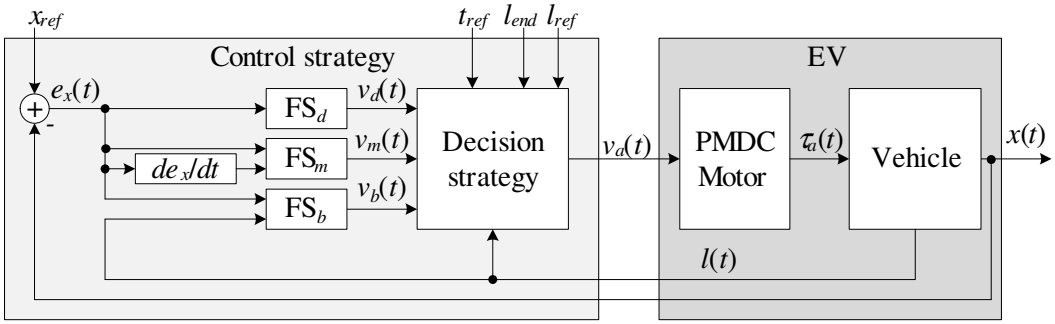

Figure 3: Structure of the electric vehicle control strategy.

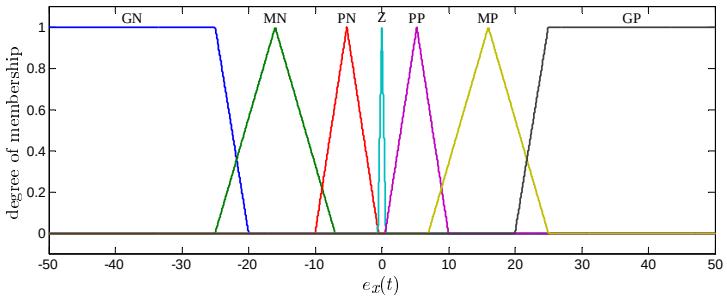

Figure 4: Membership functions of $e_x\,(t)$ for the acceleration state.

where $v_d^{min}(t)$ and $v_d^{max}(t)$ are the lower and upper limits, respectively, of the acceleration voltage. The value of the upper limit must be smaller than the nominal voltage of the motor ($v_d^{max}(t) < v_a^{nom}(t)$), t_{ref} must be smaller than the stabilization time of the system in open loop, t_{est}, ($t_{ref} < t_{est}$) e x_{ref} must be smaller than the value of the response of the system, $x(t)$, in open loop, for an input step with a value of $v_d^{min}(t)$. These three restrictions ensure the success of the acceleration state, avoiding any abrupt changes in speed.

Figure 6 llustrates the relation between the input, $e_x\,(t)$, and the output, $v_d(t)$, resulting from the rule base (Table 1) of the membership functions presented in Figures 4 and 5. This curve was obtained using the minimum in the implication step, the maximum in the aggregation step, and the centroid method in the defuzzification step. It can be seen from Figure 6 that $v_d^{min}(t) = 124\,\text{V}$ and that $v_d^{max}(t) = 135\,\text{V}$.

3.2 Fuzzy system for moving

In the case of the moving state, the fuzzy system, FS$_m(\cdot)$, uses the membership functions shown in Figures 7, 8 and 9, together with the set of rules given in Table 2.

Figures 7 and 8 illustrate the membership functions utilized for fuzzification of the input variables $e_x\,(t)$ and $de_x\,(t)$, respectively. For both input variables, seven membership functions were created (trapezoidal in the extremes and triangular in the remainder). For the output variable, $v_m(t)$, seven membership functions were created that were also trapezoidal in the extremes and triangular in the remainder, as shown in Figure 9.

It is important to note that the output variable, $v_m(t)$, does not have negative values, hence avoiding any abrupt acceleration (in routes with descents) or deceleration (in routes with ascents) due to changes in the direction of the motor.

Table 2 gives the set of fuzzy rules used in the Mamdani inference process in order to relate the input variables, $e_x\,(t)$ and $de_x\,(t)$, to the output variable, $v_m(t)$.

Figure 10 shows the relation between the inputs, $e_x\,(t)$ and $de_x\,(t)$, and the output, $v_d(t)$, resulting from the rule base (Table 2) for the membership functions shown in Figures 7, 8 and 9. This curve was obtained using the minimum in the implication step, the maximum in the aggregation step, and the centroid method in the defuzzification step.

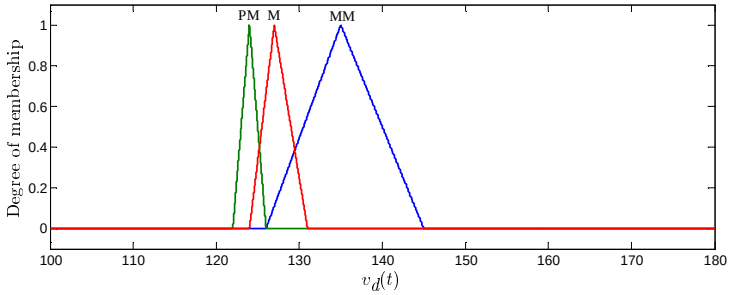

Figure 5: Membership functions of $v_d(t)$ for the acceleration state of a 220V PMDC motor.

Table 1: Set of fuzzy system rules for the acceleration state, $\text{FS}_d(\cdot)$.

$e_x\,(t)$	GN	MN	PN	Z	PP	MP	GP
	PM	PM	PM	PM	PM	M	MM

3.3 Fuzzy system for braking

The fuzzy system for braking, $\text{FS}_b(\cdot)$, consists of the membership functions shown in Figures 11, 12 and 13, together with the set of rules given in Table 3.

The input variable, $e_x(t)$, uses the same scheme described for the other fuzzy systems (FS_d and FS_m), with seven trapezoidal membership functions in the extremes and triangular functions in the remainder. The input variable, $l(t)$, (Figure 12) is composed of only two trapezoidal membership functions, representing the conditions near and far. Prior to the fuzzification process, the values of $l(t)$ are normalized using the expression

$$l_N(t) = \frac{l(t) - l_{end} + l_{ref}}{l_{ref}}, \qquad (18)$$

where $l_N(t)$ is the normalized value of $l(t)$ ranging between 0 and 1. The output variable, $v_b(t)$, consists of thirteen trapezoidal and triangular membership functions, as shown in Figure 13. In this case, the intention is to provide greater granularity in the braking process and ensure smooth deceleration.

Table 3 provides details of the set of fuzzy rules utilized in the Mamdani inference process in order to relate the input variables, $e_x(t)$ and $l_N(t)$, with the output variable, $v_b(t)$.

Figure 14 illustrates the relation between the inputs, $e_x(t)$ and $l_N(t)$, and the output, $v_b(t)$, resulting from the rule base (Table 3) for the membership functions shown in Figures 11, 12 and 13. This curve was obtained using the minimum in the implication step, the maximum in the aggregation step, and the centroid method in the defuzzification step.

4 Simulations and results

Validation of the proposed system employed simulations using the motor/gearing/vehicle model (according to the equations presented in Section 2). The values of the parameters of the PMDC motor and the vehicle are given in Tables 4 and 5, respectively. These values are based on previous field tests of electric vehicles powered by PMDC motors [26, 28].

Table 4: Parameters of the PMDC motor.

Parameter	Value
Armature resistance (R_a)	$0.1\,\Omega$
Coil inductance (L_a)	10^{-3} H
Nominal armature voltage ($v_a^{nom}(t)$)	220 V
Moment of inertia (J_m)	$0.7\,\text{Kg.m}^2$
Coefficient of viscosity (B_m)	0.08 N.m.s
Torque constant (K_τ)	1.06 N.m/A
Rate constant (K_ω)	1.06 V/rad/s
Initial rotation	100 rpm

The simulations performed using the parameters listed in Tables 4 and 5 showed that the stabilization time of the system in open loop, t_{est}, was around 19 s, and that the response of the system for an input level of $v_d^{min}(t) = 124$ V was approximately 51.6 Km/h. Hence, given the restrictions presented in Section 3.1, x_{ref} was less than 51.6 Km/h and t_{ref} was less than 19 s. Table 6 lists the values of the control strategy parameters used in the simulation.

For the acceleration step, the values of t_{ref} and x_{ref} were selected to give a longitudinal acceleration

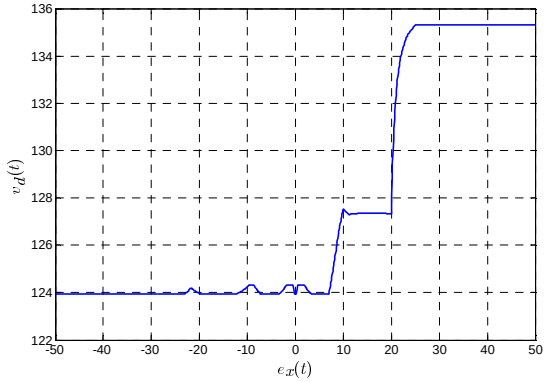

Figure 6: Relation between input and output for the rule base used in the acceleration step ($e_x\,(t) \times v_d(t)$).

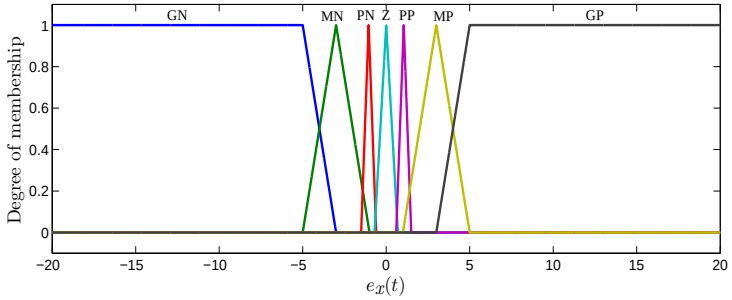

Figure 7: Membership function of the $e_x\,(t)$ variable during the moving state.

Table 5: Parameters of the vehicle.

Parameter	Value
Mass of the vehicle (M)	1500 Kg
Air density (ρ)	1.18
Coefficient of aerodynamic drag (C_d)	0.51
Frontal area (A_{fr})	2.4 m^2
Rolling resistance coefficient (C_0)	0.015
Rolling resistance coefficient (C_1)	0
Acceleration of gravity (g)	9.81 m/s^2
Wheel radius (r)	0.26 m

Table 6: Control strategy parameters used in the simulation.

Parameter	Value
Time in accelerating state (t_{ref})	7 s
Reference speed (x_{ref})	50 Km/h
Travel distance (l_{end})	10 Km
Distance to the final destination, to start the braking state (l_{ref})	25 m

of around 2 m/s^2, which is considered to be comfortable [29, 30]. In order to analyze the performance of the control strategy under adverse conditions, the simulation involved a longitudinal 10 Km route with several changes in gradient (Figure 15). The vehicle encountered two positive inclines of 10 and 15 degrees, initiated at 1 and 2.5 Km, respectively, one negative incline of 10 degrees, initiated at 5 Km, and four flat regions. The braking state was configured to begin at 25 m from the final arrival point, at 9.975 Km. The control strategy was implemented in a discrete manner, with a sampling rate of 10 ms, and the derivative of the error, $de_x\,(t)$, was estimated by difference. The simulation results obtained using the selected parameter values are shown in Figures 16, 17 and 18.

Figure 16 shows the speed of the vehicle during the acceleration state, which proceeded smoothly up to the reference speed ($x_{ref} = 50$ Km/h) in the reference time ($t_{ref} = 7$ s).

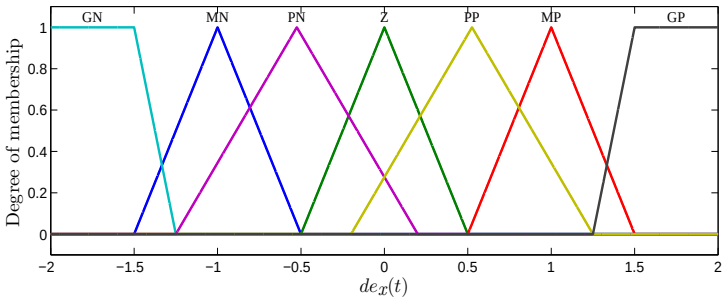

Figure 8: Membership function of the $de_x\,(t)$ variable during the moving state.

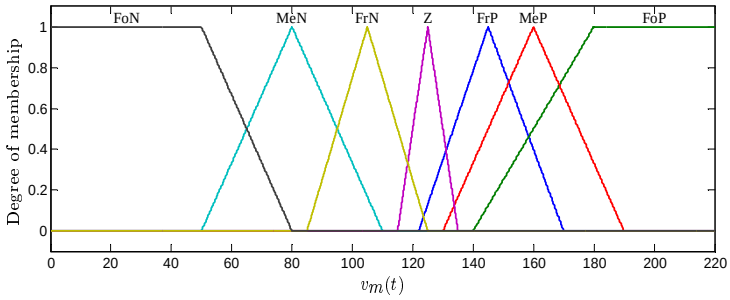

Figure 9: Membership function of the $v_m(t)$ variable during the moving state for 220V PMDC motors.

Figure 17 shows the speed of the vehicle during the moving state. It can be seen that the speed remained close to the reference speed (x_{ref}), even during changes in gradient. The error was approximately 1.2% ($x(t) = 50.61\,\mathrm{km/h}$) for the flat regions, 2.2% ($x(t) = 51.11\,\mathrm{km/h}$) for the 10 degrees negative incline, and 1.4% ($x(t) = 49.31\,\mathrm{km/h}$) and 2.7% ($x(t) = 48.64\,\mathrm{km/h}$) for the 10 and 15 degrees positive inclines, respectively. The control strategy therefore functioned effectively during the moving state, with very small changes in speed throughout the route.

Finally, Figure 18 shows the simulation results obtained for the speed of the vehicle during the braking state. The vehicle decelerated smoothly until it reached a complete halt. The braking time was around $8\,\mathrm{s}$, and the average deceleration was approximately $1.74\,\mathrm{m/s^2}$, which is a safe and comfortable value for passengers and fragile items [29, 30].

5 Conclusions

A cruise control strategy for autonomous electric vehicles was developed based on three fuzzy systems acting in parallel for three kinetic states of the vehicle (acceleration, moving, and braking). The technique offers greater precision than other systems described in the literature, and can be customized for different kinetic states, hence offering a way of improving the levels of comfort and safety for occupants and fragile objects within the vehicle.

The strategy was validated by simulation of a longitudinal vehicle powered by a permanent magnet DC motor. The results confirmed that the system complied with the configured reference criteria, enabling efficient speed control and smooth acceleration and braking. This control technique therefore has potential for use in practical applications.

References:

[1] Z. Kovacic and S. Bogdan, *Fuzzy Controller Design: Theory and Applications*. Automation and Control Engineering, Taylor & Francis, 2005.

[2] S. Haykin, *Neural Networks and Learning Machines*. No. v. 10 in Neural networks and learning machines, Prentice Hall, 2009.

[3] J. Perez, A. Gajate, V. Milanes, E. Onieva, and M. Santos, "Design and implementation of a neuro-fuzzy system for longitudinal control of autonomous vehicles," in *Fuzzy Systems (FUZZ), 2010 IEEE International Conference on*, pp. 1–6, 2010.

Table 2: Set of fuzzy system rules for the moving state, $\mathrm{FS}_m(\cdot)$.

$de_x(t)$ \ $e_x(t)$	GN	MN	PN	Z	PP	MP	GP
GN	FoN	FoN	FoN	FoN	MeN	FrN	Z
MN	FoN	FoN	FoN	MeN	FrN	Z	FrP
PN	FoN	FoN	MeN	FrN	Z	FrP	MeP
Z	FoN	MeN	FrN	Z	FrP	MeP	FoP
PP	MeN	FrN	Z	FrP	MeP	FoP	FoP
MP	FrN	Z	FrP	MeP	FoP	FoP	FoP
GP	Z	FrP	MeP	Fop	Fop	FoP	FoP

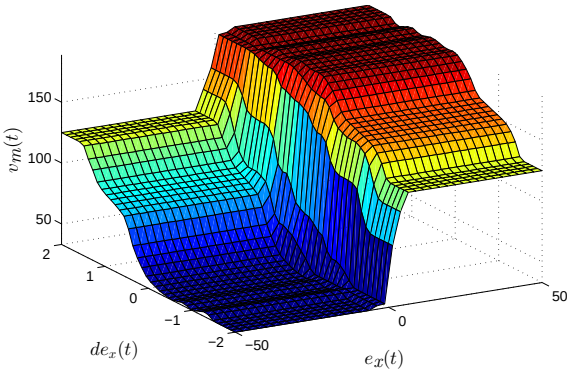

Figure 10: Relation between the inputs and output for the rule base used for the moving state, $(e_x(t), de_x(t) \times v_m(t))$.

[4] L. Cai, A. Rad, and W.-L. Chan, "An intelligent longitudinal controller for application in semi-autonomous vehicles," *Industrial Electronics, IEEE Transactions on*, vol. 57, no. 4, pp. 1487–1497, 2010.

[5] P. Ioannou and C. Chien, "Autonomous intelligent cruise control," *Vehicular Technology, IEEE Transactions on*, vol. 42, no. 4, pp. 657–672, 1993.

[6] K. S. Chang and J. S. Choi, "Automatic vehicle following using the fuzzy logic," in *Vehicle Navigation and Information Systems Conference, 1995. Proceedings. In conjunction with the Pacific Rim TransTech Conference. 6th International VNIS. 'A Ride into the Future'*, pp. 206–213, 1995.

[7] R. Verma, D. Del Vecchio, and H. Fathy, "Development of a scaled vehicle with longitudinal dynamics of an hmmwv for an its testbed," *Mechatronics, IEEE/ASME Transactions on*, vol. 13, no. 1, pp. 46–57, 2008.

[8] L. Cai, A. Rad, W. L. Chan, and M. L. Ho, "A neural-fuzzy controller for intelligent cruise control of vehicle in highways," in *Intelligent Transportation Systems, 2003. Proceedings. 2003 IEEE*, vol. 2, pp. 1389–1393 vol.2, 2003.

[9] K. E. Majdoub, F. Giri, H. Ouadi, L. Dugard, and F. Chaoui, "Vehicle longitudinal motion modeling for nonlinear control," *Control Engineering Practice*, vol. 20, no. 1, pp. 69 – 81, 2012.

[10] P. Khatun, C. Bingham, N. Schofield, and P. Mellor, "Application of fuzzy control algorithms for electric vehicle antilock braking/traction control systems," *Vehicular Technology, IEEE Transactions on*, vol. 52, no. 5, pp. 1356–1364, 2003.

[11] S. Saragioto and W. Pereira, "Lógica fuzzy aplicada ao controlador de velocidade de uma linha de montagem de eixos de veículos," in *Simpósio de Excelência em Gestão e Tecnologia*, 2012.

[12] A. Nasri, A. Hazzab, I. Bousserhane, S. Hadjeri, and P. Sicard, "Fuzzy-sliding mode speed

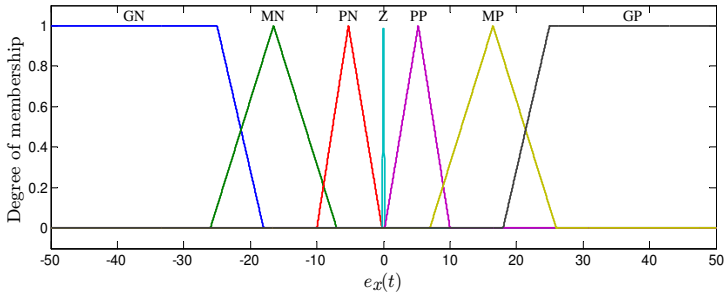

Figure 11: Membership function of the $e_x(t)$ variable during the braking state.

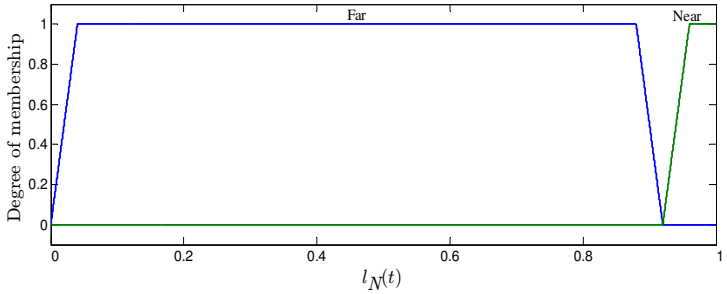

Figure 12: Membership function of the $l_N(t)$ variable during the braking state.

control for two wheels electric vehicle drive," *Journal of Electrical Engineering & Technology*, vol. 4, pp. 499–509, 2010.

[13] C. Han, J. Sul, S. Kim, Y. Lim, and J. Lee, "Development of intelligent cruise control system," in *Fuzzy Systems Conference Proceedings, 1999. FUZZ-IEEE '99. 1999 IEEE International*, vol. 1, pp. 440–443 vol.1, 1999.

[14] K. R. S. Kodagoda, W. Wijesoma, and E. Teoh, "Fuzzy speed and steering control of an agv," *Control Systems Technology, IEEE Transactions on*, vol. 10, no. 1, pp. 112–120, 2002.

[15] V. Milanes, J. Villagra, J. Perez, and C. Gonzalez, "Low-speed longitudinal controllers for mass-produced cars: A comparative study," *Industrial Electronics, IEEE Transactions on*, vol. 59, no. 1, pp. 620–628, 2012.

[16] H. Takahashi, "Automatic speed control device using self-tuning fuzzy logic," in *Automotive Applications of Electronics, 1988., IEEE Workshop on*, pp. 65–71, 1988.

[17] Z. Zalila and P. Lezy, "Longitudinal control of an autonomous vehicle through a hybrid fuzzy/classical controller," in *WESCON/94. Idea/Microelectronics. Conference Record*, pp. 118–124, 1994.

[18] R. Holve, P. Protzel, and K. Naab, "Generating fuzzy rules for the acceleration control of an adaptive cruise control system," in *Fuzzy Information Processing Society, 1996. NAFIPS., 1996 Biennial Conference of the North American*, pp. 451–455, 1996.

[19] J. Arroyabe, G. Aranguren, L. Nozal, and J. Martin, "Autonomous vehicle guidance with fuzzy algorithm," in *Industrial Electronics Society, 2000. IECON 2000. 26th Annual Confjerence of the IEEE*, vol. 3, pp. 1503–1508 vol.3, 2000.

[20] C. Hatipoglu, U. Ozguner, and M. Sommerville, "Longitudinal headway control of autonomous vehicles," in *Control Applications, 1996., Proceedings of the 1996 IEEE International Conference on*, pp. 721–726, 1996.

[21] R. Muller and G. Nocker, "Intelligent cruise control with fuzzy logic," in *Intelligent Vehicles '92 Symposium., Proceedings of the*, pp. 173–178, 1992.

[22] Z. Avdagic, E. Cernica, and S. Konjicija, "Longitudinal vehicle guidance using fuzzy logic,"

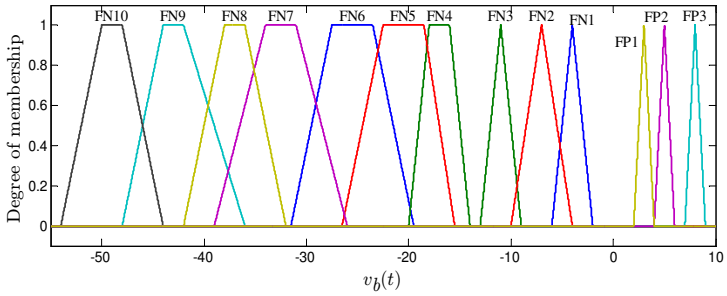

Figure 13: Membership function of the $v_b(t)$ variable during the braking state.

Table 3: Set of rules for the braking state fuzzy system, $\text{FS}_b(\cdot)$.

$l_N(t)$ \ $e_x(t)$	GN	MN	PN	Z	PP	MP	GP
Far	FN10	FN9	FN8	FN7	FN6	FN5	FN4
Near	FP1	FP2	FP3	FN3	FN3	FN2	FN1

in *Industrial Technology, 2006. ICIT 2006. IEEE International Conference on*, pp. 893–898, 2006.

[23] F. Cabello, A. Acuna, P. Vallejos, M. Orchard, and J. del Solar, "Design and validation of a fuzzy longitudinal controller based on a vehicle dynamic simulator," in *Control and Automation (ICCA), 2011 9th IEEE International Conference on*, pp. 997–1002, 2011.

[24] A. Reschka, J. Bohmer, F. Saust, B. Lichte, and M. Maurer, "Safe, dynamic and comfortable longitudinal control for an autonomous vehicle," in *Intelligent Vehicles Symposium (IV), 2012 IEEE*, pp. 346–351, 2012.

[25] H. B. Pacejka, "Tire and vehicle dynamics," *Society of Automotive Engineers and Butterworth-Heinemann*, 2002.

[26] J. Trovao, P. Pereirinha, and H. Jorge, "Simulation model and road tests comparative results of a small urban electric vehicle," in *Industrial Electronics, 2009. IECON '09. 35th Annual Conference of IEEE*, pp. 836–841, 2009.

[27] K. Ogata, *Modern Control Engineering*. Prentice Hall PTR, 2001.

[28] E. Elbakush, A. Sharaf, and I. Altas, "An efficient tri-loop controller for photovoltaic powered four-wheel electric vehicle," in *Innovations in Information Technology, 2007. IIT '07. 4th International Conference on*, pp. 421–425, 2007.

[29] A. Reschka, J. Bohmer, F. Saust, B. Lichte, and M. Maurer, "Safe, dynamic and comfortable longitudinal control for an autonomous vehicle," in *Intelligent Vehicles Symposium (IV), 2012 IEEE*, pp. 346–351, 2012.

[30] J.-J. Martinez and C. Canudas-de Wit, "A safe longitudinal control for adaptive cruise control and stop-and-go scenarios," *Control Systems Technology, IEEE Transactions on*, vol. 15, no. 2, pp. 246–258, 2007.

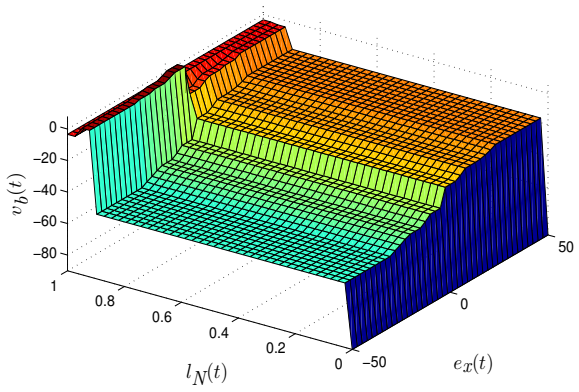

Figure 14: Relation between the inputs and the output for the rule base used for the braking state, $(e_x(t), l_N(t)) \times v_b(t)$.

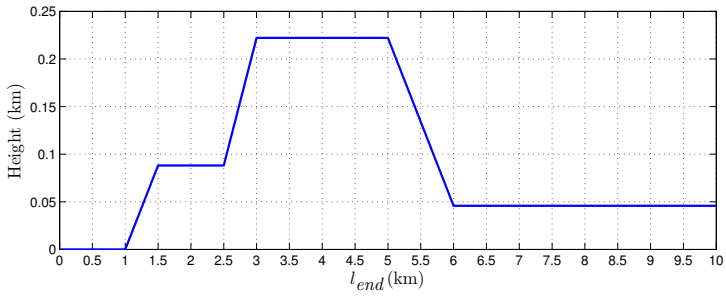

Figure 15: Route used in the simulation.

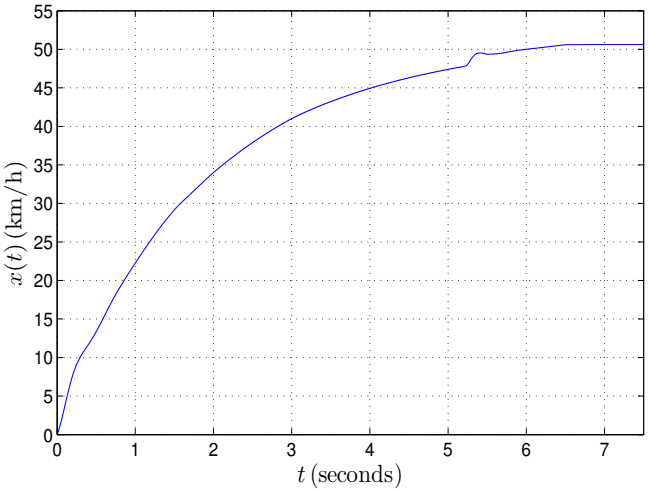

Figure 16: Simulation results for the acceleration state.

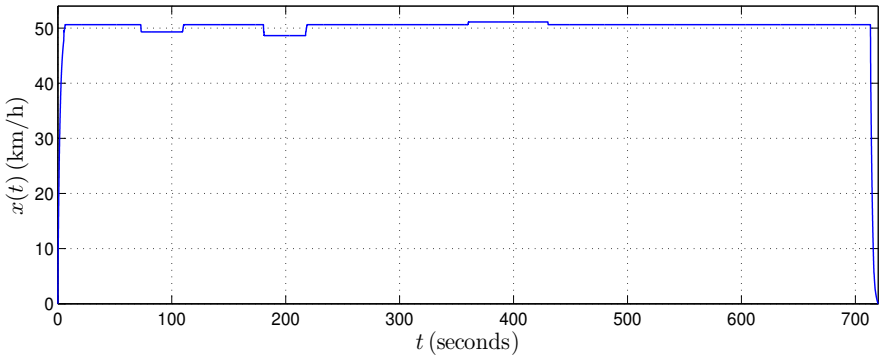

Figure 17: Simulation results for the moving state.

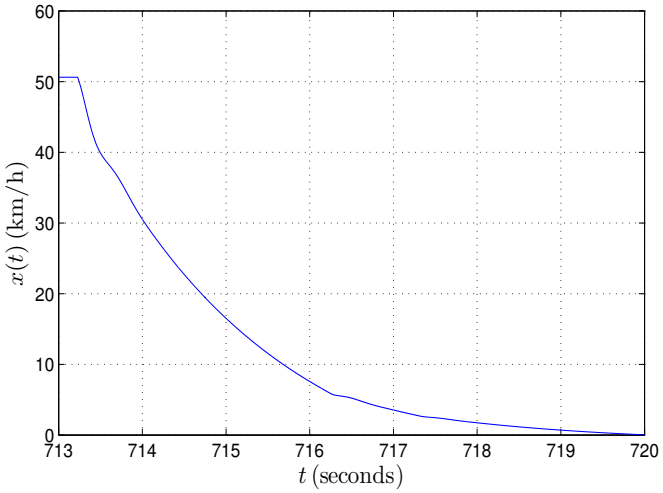

Figure 18: Simulation results for the braking state.